ADVANCED MATERIALS
www.advmat.de

Redistributing Li-Ion Flux by Parallelly Aligned Holey Nanosheets for Dendrite-Free Li Metal Anodes

*Yangen Zhou, Xiao Zhang, Yu Ding, Jiwoong Bae, Xuelin Guo, Yu Zhao, and Guihua Yu**

Li metal is the most ideal anode material to assemble rechargeable batteries with high energy density. However, nonuniform Li-ion flux during repeated Li plating and stripping leads to continuous Li dendrite growth and dead Li formation, which causes safety risks and short lifetime and thus impedes the commercialization of Li metal batteries. Here, parallelly aligned holey nanosheets on a Li metal anode are reported to simultaneously redistribute the Li-ion flux in the electrolyte and in the solid-electrolyte interphase, which allows uniform Li-ion distribution as well as fast Li-ion diffusion for reversible Li plating and stripping. With holey MgO nanosheets as an example, the protected Li anodes achieve Coulombic efficiency of ≈99% and ultralong-term reversible Li plating/stripping over 2500 h at a high current density of 10 mA cm^{-2}. A full-cell battery, using the protected anode, a 4 V Li-ion cathode, and a commercial carbonate electrolyte, shows capacity retention of 90.9% after 500 cycles.

Li metal is the ultimate anode materials for Li-ion batteries toward high energy density because of its highest theoretical specific capacity (3860 mAh g^{-1}), that is more than 10 times higher than the commercial graphite anode, and its lowest redox potential (−3.04 V vs normal hydrogen electrode) among all anode materials.[1–5] However, the practical application of Li metal anodes has long been regarded as the "Holy Grail" for high-energy-density storage systems because safety hazards and short lifetime seriously impede the progress of Li metal batteries.[6] The latest reviews present the persisting challenges and the current strategies toward the practical Li metal anodes.[7,8] Nonuniform Li-ion flux emerged in the Li plating and stripping makes Li dendrites and dead Li easy to form.[9] The Li dendrites can penetrate the separator membrane and cause a short circuit, which possibly triggers fire and explosion. At the same time, the continuous formation of dead Li including Li^+ in solid-electrolyte interphase (SEI) and electrically isolated metallic Li° consumes electrolyte and active Li metal.

Almost all commercial Li-ion batteries use carbonate electrolyte, but the SEI in situ formed on the Li metal surface in such electrolyte presents a "mosaic structure" with a heterogenous distribution of distinct components.[1,10] This structure could make the Li-ion flux nonuniform and the Li dendrites easy to grow. Electrolyte engineering, including using fluorinated solvents, high-concentration electrolytes, additives, and so on, is an effective and widely studied route to improve Li-ion flux via modifying the structure of in situ formed SEI on the Li metal.[11–15] For example, with fluoroethylene carbonate as an additive, the SEI appears to have a multilayer structure, which improves battery performance.[16] Building an artificial protective layer is another way to improve the distribution of composites in the SEI, provide fast Li-ion diffusion, and increase mechanical strength.[17–22] As effective current density can be reduced to have even current distribution by increasing the specific surface area of the current collector, the Li-ion flux for plating and stripping can be accommodated by constructing 3D conductive host.[23–27] Beyond the nonuniform Li-ion flux in the SEI, researchers are increasingly paying attention to the nonuniform Li-ion flux in the electrolyte, which may come from unevenly distributed active particles in the cathode and unevenly distributed macropores on the separator membrane. Many nanostructures were designed to redistribute the Li-ion flux in the electrolyte: modified separator, such as metal–organic framework -based separator,[28] 2D molecular brush-functionalized composite separators,[29] and solid-state fast ionic conductors coated separators;[30] 3D structure on the current collector, such as vertically aligned nanoscale channels,[31,32] vertically aligned lithiophilic nanosheets,[33,34] and 3D structure containing nanopores.[35,36] To further improve the performance of Li metal anode, both the nonuniform Li-ion flux in the electrolyte and in the SEI should be considered.

2D materials were used to construct 3D hosts or Li-ion redistributors for dendrite-free Li metal anode.[35,37,38] Holey 2D materials recently attract great attention in Li-ion batteries because of sufficient ion diffusion provided by them.[39–41] Here, we report the first kind of design based on parallelly aligned holey 2D materials on the Li metal surface to redistribute Li-ion flux both in the electrolyte and in the SEI for stabilizing Li metal anodes (**Figure 1a**). Holey nanosheets enable

Dr. Y. Zhou, X. Zhang, Dr. Y. Ding, J. Bae, X. Guo, Prof. G. Yu
Materials Science and Engineering Program, Texas Materials Institute
The University of Texas at Austin
Austin, TX 78712, USA
E-mail: ghyu@austin.utexas.edu
Prof. Y. Zhao
Institute of Functional Nano & Soft Materials (FUNSOM)
Jiangsu Key Laboratory for Carbon-Based Functional Materials & Devices
Soochow University
Suzhou, Jiangsu 215123, China
The ORCID identification number(s) for the author(s) of this article can be found under https://doi.org/10.1002/adma.202003920.

DOI: 10.1002/adma.202003920

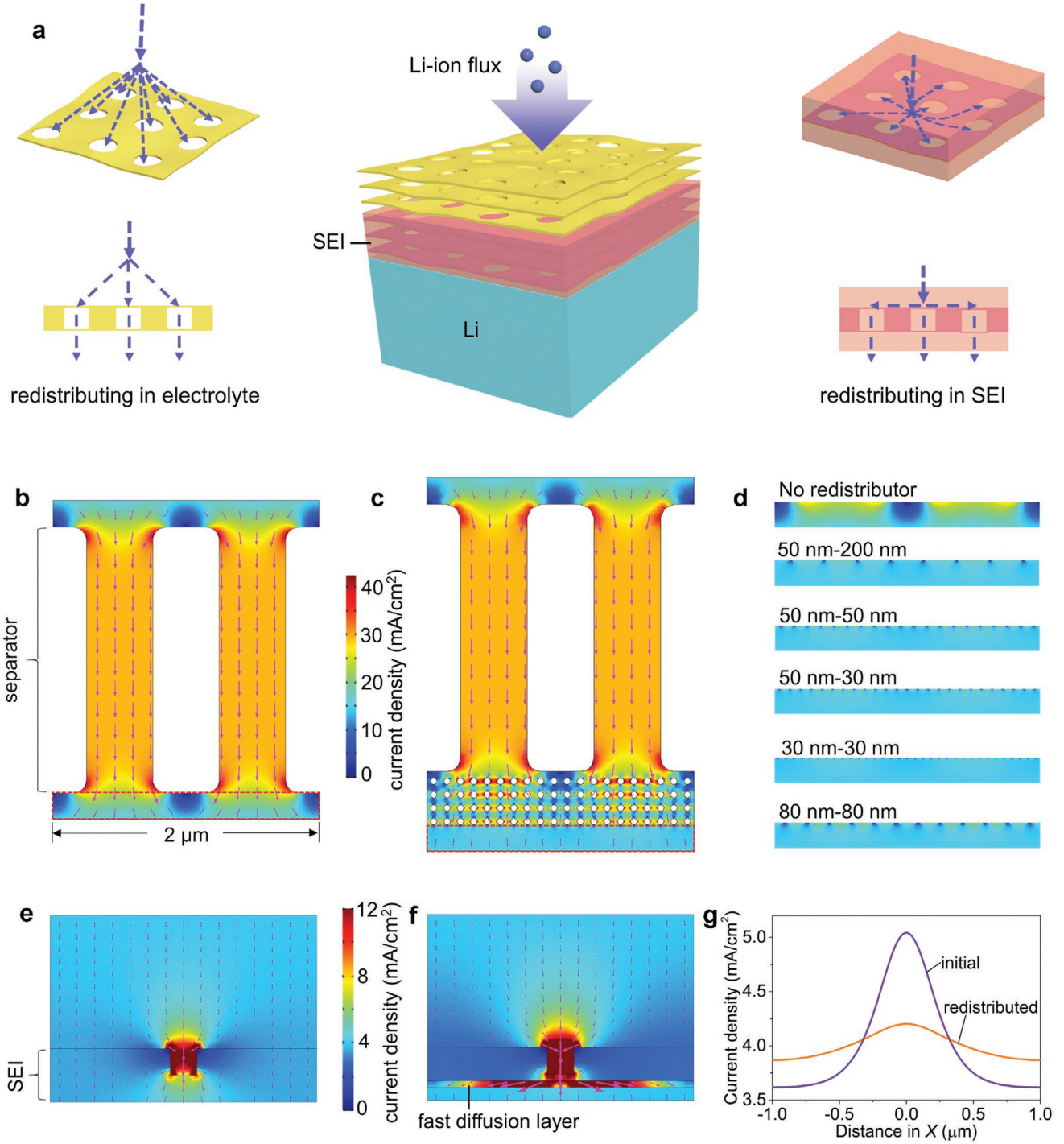

Figure 1. Simulation study of Li-ion redistribution by holey nanosheets. a) Illustration of Li-ion redistribution behavior in the parallelly aligned holey-nanosheets-protected Li metal anode. Different Li-ion diffusion coefficients in the electrolyte and in the SEI induce different redistribution behaviors. b) Simulation for nonuniform Li-ion flux in the electrolyte through a separator. c) Simulation for parallelly aligned holey nanosheets (the particle size–pore size is 50 nm–50 nm) redistributing the nonuniform Li-ion flux in electrolyte. d) Effect of particle size and pore size of the holey nanosheets on the Li-ion distribution after the redistributing process. e) Simulation for nonuniform Li-ion flux in SEI induced by a pit on the SEI surface. f) Simulation for a holey nanosheet as a fast Li-ion diffusion layer redistributing the nonuniform Li-ion flux in SEI. g) Current density distribution on Li metal surface after the Li-ion redistribution in SEI.

direct contact between electrolyte and Li metal to form multilayer SEI containing some parallelly aligned holey nanosheets. Holey nanosheets outside the SEI can redistribute the Li-ion flux in the electrolyte because of the evenly distributed pores (Figure 1a). With holey MgO nanosheets as an example, during the Li metal reducing the electrolyte to form the SEI, the holey nanosheets near the Li metal surface are lithiated into Li–Mg alloy layer with fast Li-ion diffusion to redistribute the Li-ion

flux in the SEI (Figure 1a). Different from other reported 2D material-based protective layers for Li metal anodes, the parallelly aligned holey 2D materials not only redistribute the nonuniform Li-ion flux that emerged in the electrolyte and the SEI, but also facilitate rapid Li-ion transport. It is the first time to elucidate the critical role of pores on 2D materials in regulating the Li metal anode performance. As a result, the Li metal anode achieves high Coulombic efficiency, low overpotential, and ultralong-term stability even under a high rate.

Separator membranes in rechargeable batteries prevent direct contact between anode and cathode. High porosity enables the membranes to have low resistance in batteries. For example, the commercial Celgard 2500 separator membranes are rich in irregular pores with a size range of 50–800 nm, as shown in a typical scanning electron microscopy (SEM) image in Figure S1 in the Supporting Information. The pores on the membrane are distributed nonuniformly, which may lead to nonuniform Li-ion flux. Simulation of Li-ion flux coming from the membrane for Li plating was studied with COMSOL Multiphysics (Figure S2, Supporting Information). As shown in Figure 1b, the color between Li metal anode and the separator (marked in a red box) indicates that the Li-ion flux in the electrolyte is nonuniform because of the unevenly distributed macropores on the separator. Moreover, unevenly distributed active particles in cathode also may result in the nonuniform Li-ion flux in the electrolyte for Li plating. The growth of Li dendrites would preferably occur in the regions with high current density and thus the Li dendrites can easily penetrate the separator to cause a short circuit.

In contrast, as shown in Figure 1c, after the nonuniform Li-ion flux in the electrolyte being redistributed by parallelly aligned holey 2D materials composed of interconnected 50 nm nanoparticles with uniformly distributed 50 nm pores, the Li-ion flux becomes uniform for Li plating. Figure 1d provides the distribution of current density after redistribution by the holey nanosheets with different particle sizes and different pore sizes. These simulation results reveal that either the decrease in the pore size or the decrease in the particle size can improve the uniformity of Li-ion flux. Interestingly, the nonuniform region size after the Li-ion redistribution is near the bigger one between the particle size and the pore size. However, the size of the pores on the 2D materials should be large enough for providing fast Li-ion transport. The simulation of nonuniform Li-ion flux that emerged in the SEI was also investigated, in which a pit was hypothesized on the SEI surface (Figure 1e and Figure S3, Supporting Information). The nonuniform Li-ion flux in the SEI can be generated for many reasons, such as pits, cracks, impurity particles, and so on. Therefore, the redistribution of Li-ion flux both in the electrolyte and in the SEI should be considered. As shown in Figure 1f, when the SEI containing parallelly aligned 2D nanosheet with a Li-ion diffusion coefficient much large than that of the components in common SEI, the Li-ion can be redistributed by the fast diffusion layer and become uniform for the Li plating. Figure 1g presents the distributions of current density on the Li metal surface before and after the redistribution by a fast Li-ion diffusion layer. It is observed that not only the distribution of current density becomes more uniform, but also the average current density is increased when the SEI containing the fast Li-ion diffusion layer. Increasing the layer number of the 2D holey nanosheets can further improve the uniformity of Li-ion distribution for Li plating. So, the parallelly aligned 2D materials with fast Li-ion diffusion in the SEI can redistribute the nonuniform Li-ion flux and simultaneously provide faster Li-ion transport in the SEI.

A general synthetic strategy has been demonstrated to prepare various holey metal oxides 2D materials involved a graphite oxide (GO) templating method followed by GO template removal at high temperature.[39,42] More significantly, these holey oxide nanosheets have strong mechanical stability and present minimal structural changes during lithiation/delithiation processes.[39,42] Holey MgO nanosheets are used as an example to investigate parallelly aligned holey 2D materials on the Li metal surface for redistribution of the Li-ion flux. Scanning transmission electron microscope (STEM) images show typical holey nanosheets with a lateral size of several micrometers (**Figure 2**a–c) and a pore size of ≈6.4 nm (Figure 2d), which are composed of interconnected MgO nanoparticles (Figure S4, Supporting Information) with a mean size of ≈10.5 nm (Figure 2d). The pores show irregular shape but even distribution throughout the whole nanosheets with a narrow pore size distribution. Moreover, the size of pores and nanoparticles on the nanosheets are tunable through changing the preparation parameters (Figures S5–S8, Supporting Information). Nanosheets without pores can be prepared by a similar method with a high density of interconnected nanoparticles (Figures S9 and S10, Supporting Information). Energy-dispersive X-ray spectrometry indicates that only Mg and O elements appear and are homogenously distributed on the holey nanosheets (Figure S11, Supporting Information). Atomic force microscopy (AFM) image (Figure 2e) shows that the thickness of the holey nanosheets is about 10 nm, consistent with the size of MgO nanoparticles, suggesting that the holey nanosheets are composed of monolayer MgO nanoparticles (Figure 2c). Vacuum filtration method was used in this study to assemble the holey nanosheets into a stacked 2D film with a controllable thickness on a polycarbonate filter membrane, and a press process was applied to transfer the 2D film from the filter membrane onto the Li metal surface.[17] The top-view SEM image (Figure S12, Supporting Information) shows that the Li metal surface is fully covered by parallelly aligned holey nanosheets. The packing of the holey nanosheets on Li metal presents a uniform thickness of around 500 nm, which is easily controllable (Figure 2f).

The Li metal anode protected by the parallelly aligned holey MgO nanosheets was retrieved from a symmetrical cell after 25 cycles at a current density of 1 mA cm^{-2} and an areal capacity of 1 mAh cm^{-2}. Then the composition of the protective layer as a function of depth was investigated by X-ray photoelectron spectroscopy (XPS) after Ar etching at different times (**Figure 3**). XPS spectra before Ar etching indicate that the outmost layer of the protective film is composed of MgO together with trace absorbed electrolyte, which means the holey MgO nanosheets are still on the outmost surface layer after the charge/discharge process. After Ar etching for 10 min, most of the MgO nanosheets are lithiated into Mg or Li_xMg alloy. And the product of the reaction between the electrolyte and the Li metal such as Li_2O, Li_2CO_3, LiR, and LiF, which are the common compositions of in situ formed SEI reported in the literature, are also detected.[13,43] Further increasing the etching time to 20 min, almost all the MgO nanosheets are lithiated into Li_xMg alloy. These results confirm that the parallelly aligned holey MgO nanosheets near the Li metal surface are

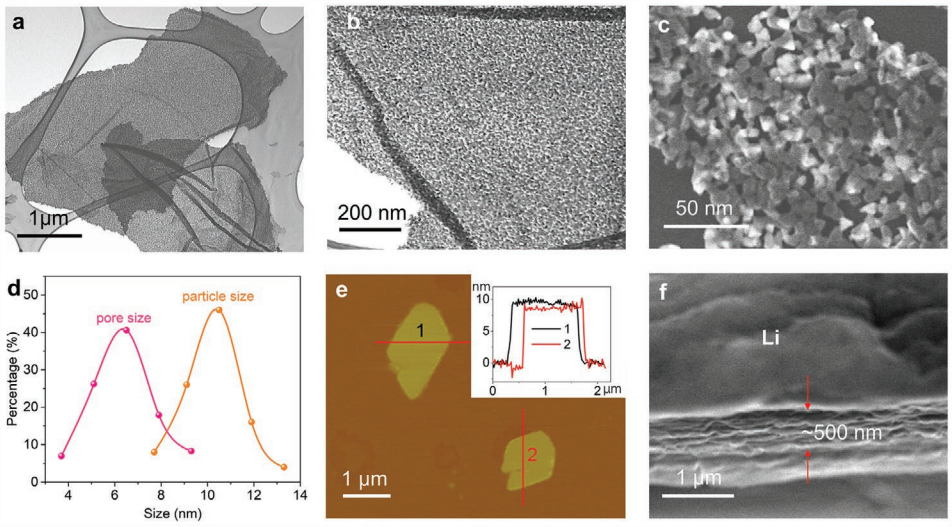

Figure 2. Parallelly aligned MgO nanosheets on Li metal. a–c) STEM and SEM images of MgO nanosheets with different magnifications. d) Distribution of particle size and pore size on the holey MgO nanosheets. e) AFM image of MgO nanosheets. f) Cross-sectional SEM image of parallelly aligned MgO nanosheets on Li metal.

lithiated into Li-rich Li–Mg alloy along with the reaction between the electrolyte and the Li metal, which results in multilayer SEI containing Li–Mg alloy nanosheets. The Li–Mg alloy can provide fast Li-ion diffusion channels because the Li diffusion energy barrier on Mg is very small (0.025 eV atom^{-1}, comparing with ≈0.14 eV atom^{-1} on Li).[18,44] The Li diffusion coefficient on

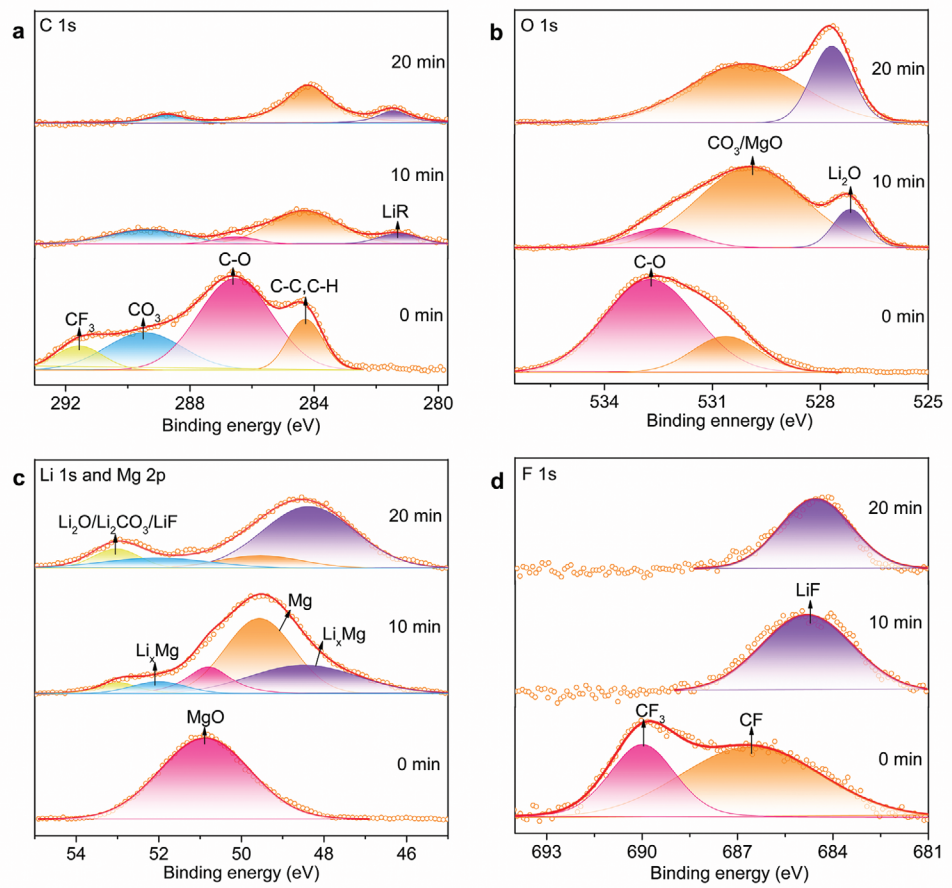

Figure 3. XPS characterization of the protective layer on Li metal surface. a–d) The C 1s (a), O 1s (b), Li 1s and Mg 2p (c), and F 1s (d) spectra after different sputtering times for the Li electrode cycled in LiTFSI electrolyte with dimethoxyethane and 1,3-dioxolane as solvent for 25 cycles.

Li–Mg alloy is ≈1×10^{-7} cm^2 s^{-1}, which far exceeds that on Li metal (5.69×10^{-11} cm^2 s^{-1}) and other conventional Li-ion electrode materials (typically $< 1 \times 10^{-10}$ cm^2 s^{-1}).[18,45] Quantitative analysis of the XPS spectra (Figure S13, Supporting Information) indicates that the amount of Li species increases when near the metallic Li surface, which benefits the Li-ion diffusion.

The electrochemical impedance spectroscopy study was applied to confirm the fast Li-ion transport provided by the holey nanosheets. For a symmetrical cell with bare Li as electrodes, the charge transfer resistance is very small initially because of fresh Li foils without SEI and gradually increases after the reaction between Li and electrolyte to form the SEI (Figure S14a, Supporting Information). For a symmetrical cell with protected Li metal as electrodes, the initial resistance is a little larger than that of the cell with bare Li (Figure S14b, Supporting Information), because the parallelly aligned holey nanosheets slow the Li-ion transport to some extent. The resistance presents a limited increase after the SEI formation because the holey nanosheets are lithiated into Li-rich alloy to enhance Li-ion diffusion in the SEI.

The symmetrical cell using bare Li electrodes has a large overpotential which reaches 170 mV after a cycling time of 180 h at a high rate (**Figure 4**a). In contrast, except for the initial cycle, the cell using the protected Li electrodes exhibits excellent stability with overpotential keeping at 50–60 mV over 2500 h, which is, to the best of our knowledge, superior to most reported Li metal anodes under similar testing conditions (Figure 4b).[12,18,28,29,46–48] The overpotential presents small fluctuations in the first 200 h probably because of the formation of new SEI after switching to high current density. And the reaction between

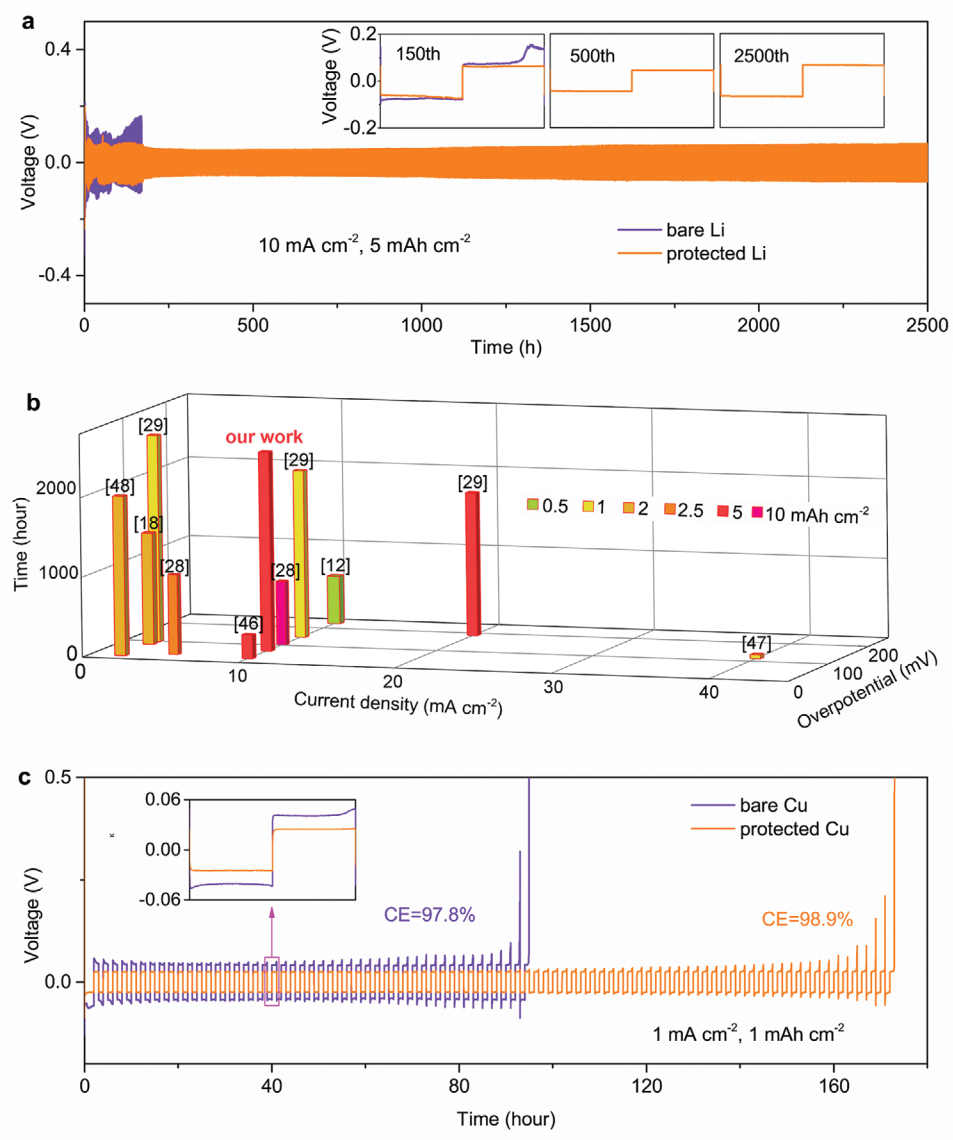

Figure 4. Electrochemical performance of MgO-protected Li metal and bare Li metal. a) Cycling performance of symmetrical cells with bare Li electrode or with protected Li electrode. b) Comparison of the cycle life of symmetric Li||Li cells with MgO-protected Li foil and that of previously reported excellent Li metal anodes stabilized by various strategies (involving refs. [12,18,28,29,46–48]). c) Coulombic efficiency of Li deposition on bare Cu electrode and on Cu electrode protected by stacked holey MgO nanosheets.

electrolyte and Li metal for increasing resistance and the lithiation of MgO for decreasing resistance occur out of sync. The Li anodes protected by parallelly aligned MgO nanosheets without pores are more stable than the bare Li anode but has a higher overpotential and worse stability than the Li anode protected by holey nanosheets in the full cell (Figure S15, Supporting Information). This is because the nanosheets outside the SEI cannot effectively redistribute the Li-ion flux in the electrolyte and does not provide sufficient Li-ion diffusion. But the holey nanosheets without pores still can redistribute the Li-ion flux in the SEI and have high shear modulus to prevent the Li dendrite penetration. When the Li metal anode is protected by the holey nanosheets with larger pore size, the symmetrical cell becomes less stable (Figure S16, Supporting Information), which confirms the influence of pore size on the redistribution of nonuniform Li-ion flux in the electrolyte. The Li metal anode protected by a thinner 2D film with a thickness of ≈200 nm could stably cycle for only 750 h (Figure S17, Supporting Information). This is because if the stacked holey nanosheets were too thin, especially thinner than the common SEI on the Li metal anode, few holey MgO nanosheets would be outside the SEI to redistribute the Li-ion flux in the electrolyte. In contrast, if the stacked holey nanosheets were too thick, the internal resistance of the cell would be increased significantly, in which potential polarization would become large. This case also increases the risk of Li dendrite growth. As a result, the symmetrical cell using Li metal anode protected by the parallelly aligned holey 2D nanosheets with a thickness of 800 nm stably cycles only ≈150 h at a high rate (Figure S18, Supporting Information). These results reveal that the Li metal anode with a thick protective layer cannot work at a high rate, but the thin artificial protective layer on Li metal anode is not easy to prepare.

The Coulombic efficiencies of the Li||Cu cells with and without parallelly aligned holey nanosheets on the Cu current collect were examined. To coat the stacked holey nanosheets on Cu, the Li metal was first pressed onto the Cu foil and rolled into a very thin film. Then the stacked holey nanosheets on the filter membrane were pressed onto the thin Li metal film. After three cycles of charge and discharge at a small current density of 1 mA cm^{-2}, the metallic Li was fully removed from the Cu foil by a Li stripping process, leaving behind only the stacked holey nanosheets and the SEI on the Cu foil. Coulombic efficiencies can be determined conveniently using exhaustive Li stripping for each cycle, but which cannot avoid the influence of side reactions between Li and Cu. This work applied a more accurate method suggested by some research groups.[49,50] 2 mAh cm^{-2} of Li was deposited onto the Cu electrode and then the cell cycled with a fixed capacity of 1 mAh cm^{-2} until the remaining Li was completely stripped to the cut-off voltage at 0.5 V. The average Coulombic efficiency for the bare Cu anode is up to 97.8%, while the value for the Cu collector protected with stacked holey nanosheets reaches ≈98.9% (Figure 4c). Moreover, the protective layer decreases the overpotential from 41 to 25 mV. As presented in the inset in Figure 4c, the overpotential for the cell with a protective layer on the Cu foil is stable, while that for the cell with bare Cu is in change with time. These results reveal that building the parallelly aligned holey MgO nanosheets on the Li metal surface is an effective method to stabilize Li metal anodes.

To demonstrate the practicability of the Li metal anodes protected by the parallelly aligned holey nanosheets, the Li metal anodes were paired with layered lithium transition metal oxide cathodes ($LiNi_{1/3}Co_{1/3}Mn_{1/3}O_2$, referred to NCM) to assemble full cells. The Coulombic efficiencies of both full cells with the bare Li and the protected Li are stabilized at 99.6% after the first 50 cycles. The full cell with the protected Li anode presents a very small capacity fade of 9.1% after 500 cycles, compared with that of 44.7% after 500 cycles for the cell with the bare Li metal anode (**Figure 5**a). The slight fluctuation of the Coulombic efficiency of the full cell with the protected Li anode after 400 cycles should be attributed to the microcracks that emerged in the NCM cathode.[51] The cracks could degrade the connectivity of grains to suddenly decrease the charge or discharge capacity, which induces the fluctuation of the Coulombic efficiency. The cracks also result in the faster performance degradation of the full cell after 400 cycles. However, the degradation rate of the full cell with protected Li anode after 400 cycles is much smaller than that of the full cell with the bare Li anode, which is attributed to the uniform Li-ion flux provided by the protected Li anode. The charge–discharge voltage profiles indicate that the voltage decay is greatly mitigated after the Li anode being protected by the holey nanosheets (Figure 5b,c). Ex situ SEM observations of the Li anodes from the full cells were conducted after 150 cycles. It is observed that abundant Li dendrites form on the bare Li metal anode (Figure 5d). In contrast, no dendrite appears on the Li anode protected by the stacked holey nanosheets (Figure 5e). It should be mentioned that such a performance, to the best of our knowledge, is the top of Li metal batteries with NCM as a cathode achieved in the commercial carbonate electrolyte (1 M $LiPF_6$ in ethylene carbonate and ethyl methyl carbonate) (Table S1, Supporting Information). Modifying the electrolyte can further improve the performance of the full cells.[13,17,52] Mg^{2+} either doped in NCM or added in the electrolyte has been reported to improve the stability of NCM cathode.[53,54] But after the addition of the holey MgO nanosheets in the electrolyte, the full cell with the bare Li anode presents negligible improvement in the performance (Figure S19, Supporting Information). Therefore, the Mg^{2+} arising from the possible dissolution of MgO in the electrolyte does not influence the performance of the full cell.

In summary, parallelly aligned holey 2D materials on the Li metal anode can redistribute nonuniform Li-ion flux both in the electrolyte and in the SEI, and simultaneously provide fast Li-ion transport, which enable a dendrite-free deposition of Li metal at a high rate and, in turn, greatly extend the cycle life of Li metal batteries. Moreover, the protection of Li metal deposition by parallelly aligned holey 2D materials is a general strategy. Because many metal oxides can be lithiated to form Li-rich alloy particles with a fast Li-ion diffusion coefficient.[18,44,55,56] The holey nanosheet structure of these metal oxides can be prepared by the same GO-template method reported here, taking ZnO as another example (Figures S20–S22, Supporting Information). Uniform and dendrite-free deposition of Li metals at high deposition capacity and high rate can be observed with parallelly aligned holey ZnO nanosheets as the protective film (Figure S23 and Table S2, Supporting Information). This work opens up the systematic engineering on the redistribution of

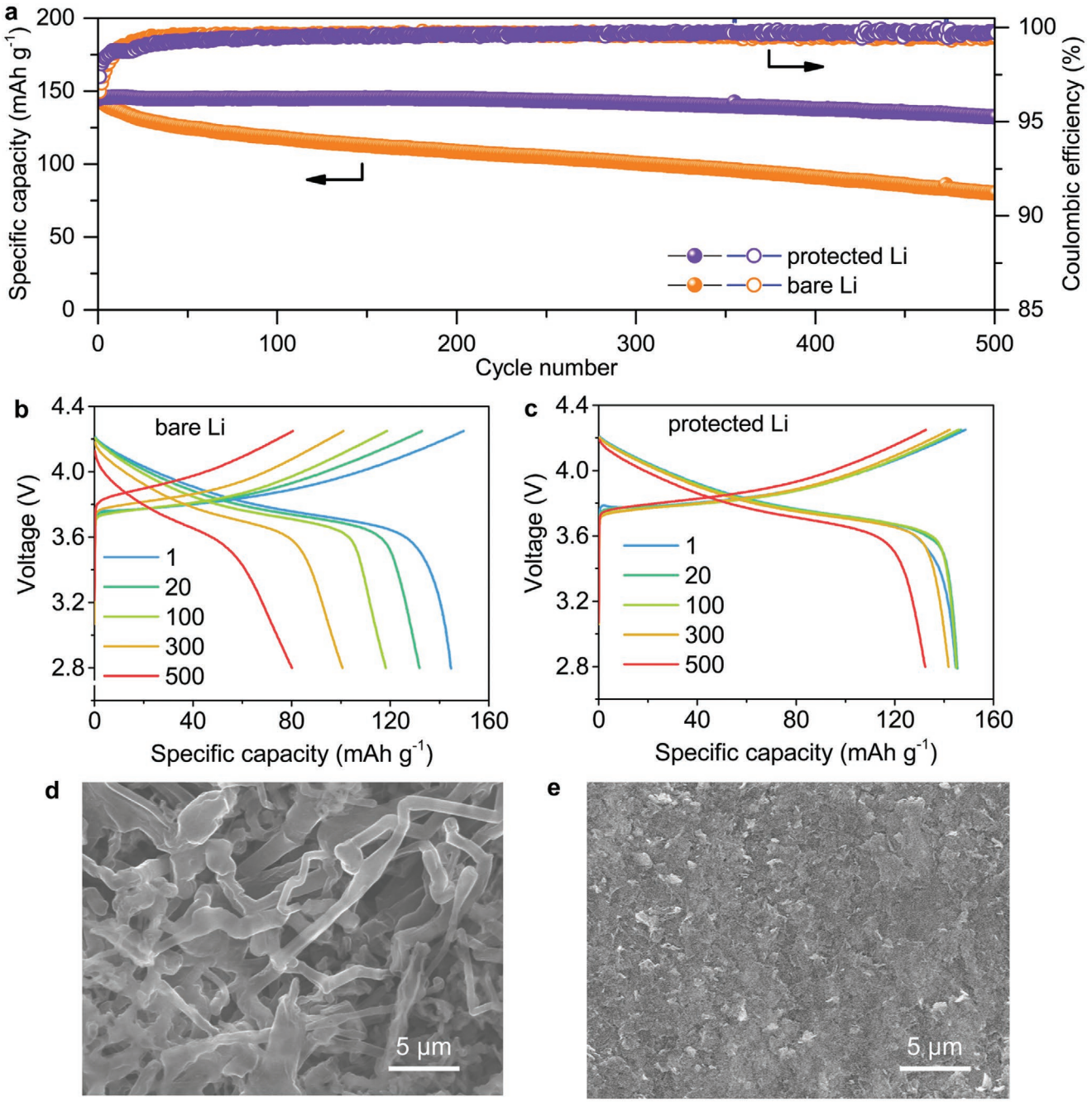

Figure 5. Electrochemical performance of Li||NCM full cells. a) Capacity retention with cycle numbers of cells at 1 C. b,c) Charge and discharge voltage profiles for the full cells without (b) and with (c) protection. d,e) Morphology of Li metal anodes after 150 cycles without (d) and with (e) protection.

Li-ion flux based on holey 2D materials to endow the Li metal anodes with excellent cycling performance at high rate with high areal capacity.

Supporting Information

Supporting Information is available from the Wiley Online Library or from the author.

Acknowledgements

G.Y. acknowledges the financial support from Welch Foundation award F-1861, Sloan Research Fellowship, and Camille Dreyfus Teacher-Scholar Award. Y.Z. acknowledges the financial support of the National Natural Science Foundation of China (51772199), the Collaborative Innovation Centre of Suzhou Nano Science & Technology (NANO-CIC), the Base for Introducing Talents of Discipline to Universities (National 111 Project), and the Priority Academic Program Development of Jiangsu Higher Education Institutions.

Conflict of Interest

The authors declare no conflict of interest.

Keywords

holey nanosheets, ion redistributors, Li-ion flux, Li metal anodes, Li-rich alloys

Received: June 8, 2020
Revised: July 6, 2020
Published online: August 12, 2020

[1] X.-B. Cheng, R. Zhang, C.-Z. Zhao, Q. Zhang, *Chem. Rev.* **2017**, *117*, 10403.
[2] B. Liu, J.-G. Zhang, W. Xu, *Joule* **2018**, *2*, 833.
[3] W. Xu, J. Wang, F. Ding, X. Chen, E. Nasybulin, Y. Zhang, J.-G. Zhang, *Energy Environ. Sci.* **2014**, *7*, 513.
[4] R. Zhang, N. W. Li, X. B. Cheng, Y. X. Yin, Q. Zhang, Y. G. Guo, *Adv. Sci.* **2017**, *4*, 1600445.
[5] A. Zhamu, G. Chen, C. Liu, D. Neff, Q. Fang, Z. Yu, W. Xiong, Y. Wang, X. Wang, B. Z. Jang, *Energy Environ. Sci.* **2012**, *5*, 5701.
[6] D. Lin, Y. Liu, Y. Cui, *Nat. Nanotechnol.* **2017**, *12*, 194.
[7] Y. Zhang, T.-T. Zuo, J. Popovic, K. Lim, Y.-X. Yin, J. Maier, Y.-G. Guo, *Mater. Today* **2020**, *33*, 56.
[8] X. Zhang, Y. Yang, Z. Zhou, *Chem. Soc. Rev.* **2020**, *49*, 3040.
[9] X.-B. Cheng, R. Zhang, C.-Z. Zhao, F. Wei, J.-G. Zhang, Q. Zhang, *Adv. Sci.* **2016**, *3*, 1500213.
[10] D. Wang, W. Zhang, W. Zheng, X. Cui, T. Rojo, Q. Zhang, *Adv. Sci.* **2017**, *4*, 1600168.
[11] M. D. Tikekar, S. Choudhury, Z. Tu, L. A. Archer, *Nat. Energy* **2016**, *1*, 16114.
[12] J. Qian, W. A. Henderson, W. Xu, P. Bhattacharya, M. Engelhard, O. Borodin, J.-G. Zhang, *Nat. Commun.* **2015**, *6*, 6362.
[13] J. Zheng, M. H. Engelhard, D. Mei, S. Jiao, B. J. Polzin, J.-G. Zhang, W. Xu, *Nat. Energy* **2017**, *2*, 17012.
[14] X.-Q. Zhang, X.-B. Cheng, X. Chen, C. Yan, Q. Zhang, *Adv. Funct. Mater.* **2017**, *27*, 1605989.
[15] J.-Y. Hwang, S.-J. Park, C. S. Yoon, Y.-K. Sun, *Energy Environ. Sci.* **2019**, *12*, 2174.
[16] Y. Li, Y. Li, A. Pei, K. Yan, Y. Sun, C.-L. Wu, L.-M. Joubert, R. Chin, A. L. Koh, Y. Yu, J. Perrino, B. Butz, S. Chu, Y. Cui, *Science* **2017**, *358*, 506.
[17] M. S. Kim, J.-H. Ryu, Deepika, Y. R. Lim , I. W. Nah, K.-R. Lee, L. A. Archer, W. Il Cho, *Nat. Energy* **2018**, *3*, 889.
[18] X. Liang, Q. Pang, I. R. Kochetkov, M. S. Sempere, H. Huang, X. Sun, L. F. Nazar, *Nat. Energy* **2017**, *2*, 17119.
[19] Y. Gao, Z. Yan, J. L. Gray, X. He, D. Wang, T. Chen, Q. Huang, Y. C. Li, H. Wang, S. H. Kim, T. E. Mallouk, D. Wang, *Nat. Mater.* **2019**, *18*, 384.
[20] Y. Gu, W.-W. Wang, Y.-J. Li, Q.-H. Wu, S. Tang, J.-W. Yan, M.-S. Zheng, D.-Y. Wu, C.-H. Fan, W.-Q. Hu, Z.-B. Chen, Y. Fang, Q.-H. Zhang, Q.-F. Dong, B.-W. Mao, *Nat. Commun.* **2018**, *9*, 1339.
[21] G. Zheng, S. W. Lee, Z. Liang, H.-W. Lee, K. Yan, H. Yao, H. Wang, W. Li, S. Chu, Y. Cui, *Nat. Nanotechnol.* **2014**, *9*, 618.
[22] N. W. Li, Y. X. Yin, C. P. Yang, Y. G. Guo, *Adv. Mater.* **2016**, *28*, 1853.
[23] G. Li, Z. Liu, Q. Huang, Y. Gao, M. Regula, D. Wang, L.-Q. Chen, D. Wang, *Nat. Energy* **2018**, *3*, 1076.
[24] D. Lin, Y. Liu, Z. Liang, H.-W. Lee, J. Sun, H. Wang, K. Yan, J. Xie, Y. Cui, *Nat. Nanotechnol.* **2016**, *11*, 626.
[25] J. Xie, J. Wang, H. R. Lee, K. Yan, Y. Li, F. Shi, W. Huang, A. Pei, G. Chen, R. Subbaraman, J. Christensen, Y. Cui, *Sci. Adv.* **2018**, *4*, eaat5168.
[26] Z. Liang, D. Lin, J. Zhao, Z. Lu, Y. Liu, C. Liu, Y. Lu, H. Wang, K. Yan, X. Tao, Y. Cui, *Proc. Natl. Acad. Sci. USA* **2016**, *113*, 2862.
[27] R. Zhang, X.-B. Cheng, C.-Z. Zhao, H.-J. Peng, J.-L. Shi, J.-Q. Huang, J. Wang, F. Wei, Q. Zhang, *Adv. Mater.* **2016**, *28*, 2155.
[28] S. Bai, Y. Sun, J. Yi, Y. He, Y. Qiao, H. Zhou, *Joule* **2018**, *2*, 2117.
[29] C. Li, S. Liu, C. Shi, G. Liang, Z. Lu, R. Fu, D. Wu, *Nat. Commun.* **2019**, *10*, 1363.
[30] C.-Z. Zhao, P.-Y. Chen, R. Zhang, X. Chen, B.-Q. Li, X.-Q. Zhang, X.-B. Cheng, Q. Zhang, *Sci. Adv.* **2018**, *4*, eaat3446.
[31] W. Liu, D. Lin, A. Pei, Y. Cui, *J. Am. Chem. Soc.* **2016**, *138*, 15443.
[32] S. H. Wang, Y. X. Yin, T. T. Zuo, W. Dong, J. Y. Li, J. L. Shi, C. H. Zhang, N. W. Li, C. J. Li, Y. G. Guo, *Adv. Mater.* **2017**, *29*, 1703729.
[33] C. Zhang, W. Lv, G. Zhou, Z. Huang, Y. Zhang, R. Lyu, H. Wu, Q. Yun, F. Kang, Q.-H. Yang, *Adv. Energy Mater.* **2018**, *8*, 1703404.
[34] J. Luan, Q. Zhang, H. Yuan, D. Sun, Z. Peng, Y. Tang, X. Ji, H. Wang, *Adv. Sci.* **2019**, *6*, 1901433.
[35] Y. Guo, P. Niu, Y. Liu, Y. Ouyang, D. Li, T. Zhai, H. Li, Y. Cui, *Adv. Mater.* **2019**, *31*, 1900342.
[36] Z. Jiang, T. Liu, L. Yan, J. Liu, F. Dong, M. Ling, C. Liang, Z. Lin, *Energy Storage Mater.* **2018**, *11*, 267.
[37] C. Zhang, A. Wang, J. Zhang, X. Guan, W. Tang, J. Luo, *Adv. Energy Mater.* **2018**, *8*, 1802833.
[38] D. Zhang, S. Wang, B. Li, Y. Gong, S. Yang, *Adv. Mater.* **2019**, *31*, 1901820.
[39] L. Peng, P. Xiong, L. Ma, Y. Yuan, Y. Zhu, D. Chen, X. Luo, J. Lu, K. Amine, G. Yu, *Nat. Commun.* **2017**, *8*, 15139.
[40] H. Sun, L. Mei, J. Liang, Z. Zhao, C. Lee, H. Fei, M. Ding, J. Lau, M. Li, C. Wang, X. Xu, G. Hao, B. Papandrea, I. Shakir, B. Dunn, Y. Huang, X. Duan, *Science* **2017**, *356*, 599.
[41] L. Peng, Z. Fang, Y. Zhu, C. Yan, G. Yu, *Adv. Energy Mater.* **2018**, *8*, 1702179.
[42] D. Chen, L. Peng, Y. Yuan, Y. Zhu, Z. Fang, C. Yan, G. Chen, R. Shahbazian-Yassar, J. Lu, K. Amine, G. Yu, *Nano Lett.* **2017**, *17*, 3907.
[43] Q. Pang, A. Shyamsunder, B. Narayanan, C. Y. Kwok, L. A. Curtiss, L. F. Nazar, *Nat. Energy* **2018**, *3*, 783.
[44] Z. Tu, S. Choudhury, M. J. Zachman, S. Wei, K. Zhang, L. F. Kourkoutis, L. A. Archer, *Nat. Energy* **2018**, *3*, 310.
[45] Y. Zhang, K. S. R. Chandran, M. Jagannathan, H. Z. Bilheux, J. C. Bilheux, *J. Electrochem. Soc.* **2017**, *164*, A28.
[46] E. Cha, M. D. Patel, J. Park, J. Hwang, V. Prasad, K. Cho, W. Choi, *Nat. Nanotechnol.* **2018**, *13*, 337.
[47] P. Xue, S. Liu, X. Shi, C. Sun, C. Lai, Y. Zhou, D. Sui, Y. Chen, J. Liang, *Adv. Mater.* **2018**, *30*, 1804165.
[48] R. V. Salvatierra, G. A. Lopez-Silva, A. S. Jalilov, J. Yoon, G. Wu, A. L. Tsai, J. M. Tour, *Adv. Mater.* **2018**, *30*, 1803869.
[49] K.-H. Chen, A. J. Sanchez, E. Kazyak, A. L. Davis, N. P. Dasgupta, *Adv. Energy Mater.* **2019**, *9*, 1802534.
[50] B. D. Adams, J. Zheng, X. Ren, W. Xu, J.-G. Zhang, *Adv. Energy Mater.* **2018**, *8*, 1702097.
[51] H. Liu, M. Wolf, K. Karki, Y.-S. Yu, E. A. Stach, J. Cabana, K. W. Chapman, P. J. Chupas, *Nano Lett.* **2017**, *17*, 3452.
[52] X. Cao, X. Ren, L. Zou, M. H. Engelhard, W. Huang, H. Wang, B. E. Matthews, H. Lee, C. Niu, B. W. Arey, Y. Cui, C. Wang, J. Xiao, J. Liu, W. Xu, J.-G. Zhang, *Nat. Energy* **2019**, *4*, 796.
[53] Z. Huang, Z. Wang, X. Zheng, H. Guo, X. Li, Q. Jing, Z. Yang, *Electrochim. Acta* **2015**, *182*, 795.
[54] R. Wagner, V. Kraft, B. Streipert, J. Kasnatscheew, D. R. Gallus, M. Amereller, M. Korth, I. Cekic-Laskovic, M. Winter, *Electrochim. Acta* **2017**, *228*, 9.
[55] Q. Pang, X. Liang, I. R. Kochetkov, P. Hartmann, L. F. Nazar, *Angew. Chem., Int. Ed.* **2018**, *57*, 9795.
[56] K. Liao, S. Wu, X. Mu, Q. Lu, M. Han, P. He, Z. Shao, H. Zhou, *Adv. Mater.* **2018**, *30*, 1705711.